Inelastic neutron scattering and muon spin relaxation investigations of the deuterated Kondo lattices CeNiSnD$_x$

X. Y. Zheng,[1] D. T. Adroja [●],[2,3,*] B. Chevalier,[4] Z. Y. Shan,[1] A. D. Hillier,[2] H. Q. Yuan,[1,5,6] and M. Smidman [●][1,†]

[1]*Center for Correlated Matter and School of Physics, Zhejiang University, Hangzhou 310058, China*

[2]*ISIS Facility, STFC Rutherford Appleton Laboratory, Chilton, Oxfordshire OX11 0QX, United Kingdom*

[3]*Highly Correlated Matter Research Group, Physics Department, University of Johannesburg,*
P.O. Box 524, Auckland Park 2006, South Africa

[4]*ICMCB, CNRS (UPR 9048), Avenue du Dr. A. Schweitzer, 33608 Pessac, France*

[5]*Collaborative Innovation Center of Advanced Microstructures, Nanjing 210093, China*

[6]*State Key Laboratory of Silicon Materials, Zhejiang University, Hangzhou 310058, China*

CeNiSn is a Kondo semimetal where a gap opens at low temperatures due to hybridization between $4f$ and conduction electrons, but a full insulating state fails to develop. Upon the insertion of hydrogen, long-range magnetic order is induced. Here we report zero-field muon spin relaxation and inelastic neutron scattering measurements of polycrystalline samples of the deuterides CeNiSnD$_x$ (x=1.0, 1.8). The muon spin relaxation results confirm magnetic ordering in the whole sample of CeNiSnD below around 4.7 K, while inelastic neutron scattering reveals two well-defined crystalline-electric field (CEF) excitations at around 13 and 34 meV in CeNiSnD, and 5 and 27 meV for CeNiSnD$_{1.8}$. These results suggest that hydrogenation leads to the localization of the Ce-$4f$ electrons, giving rise to long-range magnetic order. We propose CEF level schemes for both systems, which predict a ground-state moment of $0.96\mu_B$/Ce within the ab plane for CeNiSnD$_{1.8}$ and a saturated moment of $1.26\mu_B$/Ce along the easy c axis for CeNiSnD, that account for the observed magnetic properties.

I. INTRODUCTION

Ce-based Kondo lattices can exhibit various electronic phases arising from competition between the Ruderman-Kittel-Kasuya-Yosida (RKKY) interaction and the Kondo effect, including complex magnetic order, unconventional superconductivity, strange metal behavior, and quantum criticality [1–3]. The relative strengths of these interactions can be adjusted by nonthermal parameters such as hydrostatic pressure, magnetic fields, and chemical doping, which can often readily tune the ground states of Kondo lattice systems. Hydrogenation is one such means of tuning Kondo lattices, whereby the insertion of hydrogen generally expands the lattice, corresponding to a negative chemical pressure which decreases the hybridization strength. This can either induce magnetic ordering in otherwise nonmagnetic heavy fermions [4–6] or tune the ordering temperatures of Kondo magnets [7,8]. On the other hand, strong bonding between the rare-earth and hydrogen ions can modify the electronic structure, resulting in the delocalization of Ce-$4f$ electrons, and change the ground state from magnetic ordering to one with spin fluctuations or intermediate valence [9–12].

CeNiSn is an unusual heavy-fermion system, whereby transport measurements evidence the opening of a gap due to Kondo hybridization between the $4f$ and conduction electrons, but a full Kondo insulating state fails to develop [13–16], which had been ascribed to a V-shaped density of states at the Fermi level arising from highly anisotropic or even nodal Kondo hybridization [17–22]. Furthermore, no magnetic ordering is detected down to 0.1 K, also evidencing a strong Kondo effect [23]. Recently, CeNiSn was also proposed to be a topological Kondo semimetal with Möbius-twisted surface states [24,25], while the high-temperature band structure may also correspond to a Dirac nodal-loop semimetal with hourglass-type bulk band crossings [26,27].

Meanwhile, inelastic neutron scattering (INS) at low temperatures reveals unusual magnetic excitations together with a spin gap that appear to exist only at certain momentum transfers **Q** [28–30], and it is not settled whether these primarily correspond to antiferromagnetic correlations [29,30], interband transitions from the heavy renormalized Fermi surface with a partial hybridization gap [21,31], or, alternatively, a heavy-fermion spin liquid arising due to hybridization between crystalline-electric field (CEF) excitations and conduction electrons [32,33]. Moreover, an additional magnetic excitation was detected in CeNiSn at higher-energy transfers of around 40 meV [34,35], which may correspond to a CEF excitation broadened by the Kondo hybridization, while doping with Cu, Pd, and Pt for Ni leads to the appearance of two well-defined CEF excitations [36–38].

Two hydrides derived from CeNiSn have been reported, CeNiSnH and CeNiSnH$_{1.8}$, where CeNiSnH has the same orthorhombic TiNiSi-type structure as CeNiSn and orders antiferromagnetically below 4.5–5.1 K [39–41], while

*Corresponding author: devashibhai.adroja@stfc.ac.uk
†Corresponding author: msmidman@zju.edu.cn

CeNiSnH$_{1.8}$ has a hexagonal ZrBeSi-type structure and has a ferromagnetic transition at $T_C = 7$ K [39,42]. In both cases, hydrogenation induces a small expansion of the unit cell volume, leading to magnetic ordering, while the influence of the Kondo interaction can be inferred by the reduced magnetic entropy at the ordering temperature. This influence is more prominent in CeNiSnH$_{1.8}$ than CeNiSnH since the former also exhibits a Kondo-like increase of the resistivity with decreasing temperature and has a larger Sommerfeld coefficient γ_{ele} [39]. The ordered magnetic moment of CeNiSnH is estimated to be $1.37\mu_B$/Ce along the c axis from neutron diffraction [41]. The relatively small ordered moments in rare-earth compounds may be due to the reduced moments of the ground-state Kramers doublet arising from the splitting of the ground-state $J = 5/2$ multiplet, while Kondo hybridization can further reduce the values. Disentangling these effects requires probing the CEF excitations and determining the CEF level schemes.

It is therefore of particular interest to characterize the magnetic properties of CeNiSnH and CeNiSnH$_{1.8}$ using microscopic techniques, and in particular to understand the evolution of the magnetic excitations and electronic ground state of hydrogenated CeNiSnH$_x$. Here we report inelastic neutron scattering measurements on polycrystalline samples of CeNiSnD and CeNiSnD$_{1.8}$, as well as muon spin relaxation (μSR) measurements of CeNiSnD. The μSR measurements confirm long-range magnetic order in CeNiSnD, where the whole sample volume orders magnetically below T_N. INS reveals well-defined CEF excitations in both CeNiSnD and CeNiSnD$_{1.8}$, demonstrating that hydrogenation leads to a localization of the Ce-$4f$ electrons in CeNiSn, and CEF level schemes are proposed.

II. EXPERIMENTAL DETAILS

INS and μSR measurements were performed on powder samples of CeNiSnD$_x$ ($x = 1, 1.8$) at the ISIS facility at the Rutherford Appleton Laboratory, UK. Note that deuterated, rather than hydrogenated, samples were utilized due to the much larger incoherent neutron scattering cross section of hydrogen. INS were measured using the HET time-of-flight chopper spectrometer with incident neutron energies of 20 and 60 meV. On HET, neutrons are scattered from the sample into two forward detector banks at low scattering angles covering $2.4° \rightarrow 6.9°$ and $9.0° \rightarrow 29.0°$, and banks at $110.2° \rightarrow 119.2°$ and $125.1° \rightarrow 138.4°$ at high scattering angles. In order to estimate the phonon contribution to the scattering of CeNiSnD$_{1.8}$, isostructural LaNiSnD$_{1.8}$ was also measured, while the phonon contribution for CeNiSnD was estimated from INS measurements of LaNiSn [36]. The magnetic contributions to the INS were fitted to a CEF model using MANTID [43].

III. RESULTS AND DISCUSSION

A. Zero-field μSR measurements

Zero-field (ZF) muon spin relaxation measurements of CeNiSnD at selected temperatures are displayed in Fig. 1(a). At lower temperatures, there is a significant drop in the asymmetry, consistent with the onset of long-range magnetic
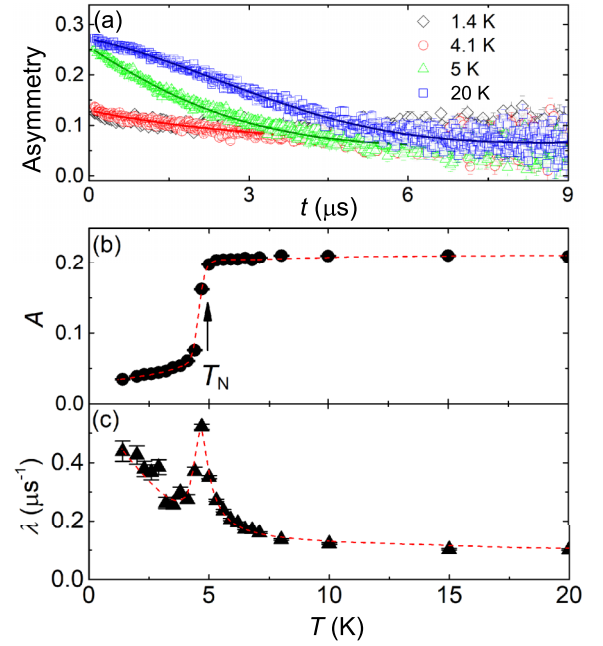

FIG. 1. (a) Zero-field μSR spectra of CeNiSnD measured at four temperatures, both above and below the magnetic transition. The solid lines correspond to the fitting using Eq. (1), where (b) shows the temperature dependence of the initial asymmetry A of the component corresponding to the sample and (c) shows the Lorentzian relaxation rate λ. The red dashed lines in (b) and (c) are guides to the eye.

order. We do not observe signatures of coherent oscillations in the asymmetry below T_N, indicating that the local magnetic fields at the muon stopping site are too large for the corresponding oscillations to be resolved. Note that the width of the implanted muon pulse is around 80 ns at the ISIS Facility (compared to a time width of <1 ns for the continuous muon beam at the Paul Scherrer Institut), meaning that frequencies above around 10 MHz cannot be resolved. Since the spins of the implanted muons precess at the Larmor frequency associated with the perpendicular component of the local magnetic field, coherent oscillations associated with internal fields above around ~700 G will not be detected. On the other hand, coherent oscillations are observed in μSR measurements of both CeNiSnH and CeNiSnH$_{1.8}$ using a continuous muon source, which has much greater time resolution and allows measurements of GHz frequencies and fast relaxation rates (>100 μs^{-1}) [44].

The asymmetry was fitted to a damped Gaussian Kubo-Toyabe (KT) function,

$$G_{ZF}(t) = A\left[\frac{1}{3} + \frac{2}{3}(1 - \delta^2 t^2)\exp\left(-\frac{\delta^2 t^2}{2}\right)\right]$$
$$\times \exp(-\lambda t) + A_{bg}, \quad (1)$$

where A is the initial asymmetry, A_{bg} corresponds to the time-independent background term from muons stopping in the silver sample holder, while δ and λ are the Gaussian and exponential relaxation rates, respectively. The value of δ was fixed from fitting the data at 20 K, while the temperature

dependence of the fitted A is displayed in Fig 1(b). There is a sharp drop in A below 5 K, which decreases to a value of around one-third of that at high temperatures. Such a loss of asymmetry in measurements of polycrystalline samples strongly suggests that the whole sample magnetically orders below the magnetic transition. There is also a sharp peak in λ at 4.7 K [Fig. 1(c)], which is consistent with the critical slowing down of spin fluctuations upon approaching the transition.

B. Inelastic neutron scattering

1. CeNiSnD$_{1.8}$

The inelastic neutron scattering responses of CeNiSnD$_{1.8}$ and the nonmagnetic analog LaNiSnD$_{1.8}$ measured with an incident energy $E_i = 60$ meV at 7 K are shown as color-coded intensity plots in Figs. 2(a) and 2(b), respectively, while the responses with $E_i = 20$ meV at $T = 7$ K are shown in Figs. 2(c) and 2(d). A clear dispersionless excitation is observed at around 27 meV, while there is only very weak intensity at this energy transfer for LaNiSnD$_{1.8}$, and therefore this can be ascribed to be a crystalline-electric field excitation of the Ce^{3+} ions. There is also additional intensity at low momentum transfers $|\mathbf{Q}|$ at low energy close to the elastic line in CeNiSnD$_{1.8}$, which corresponds to magnetic scattering. This can be clearly seen from a comparison of the cuts integrated over low $|\mathbf{Q}|$, corresponding to momentum ranges of 0–4 Å^{-1} for $E_i = 60$ meV and 0–2.5 Å^{-1} for $E_i = 20$ meV, displayed in Figs. 2(e) and 2(f), respectively, where the intensity of the CeNiSnD$_{1.8}$ data exceeds that of LaNiSnD$_{1.8}$ both in the vicinity of the 27 meV excitation and below 10 meV. On the other hand, Figs. 2(g) and 2(h) show cuts obtained from integrating over high $|\mathbf{Q}|$, for $E_i = 60$ meV (6–10 Å^{-1}) and $E_i = 20$ meV (3.5–6 Å^{-1}), respectively. It can be seen that these cuts are very similar between CeNiSnD$_{1.8}$ and LaNiSnD$_{1.8}$, suggesting very similar phonon spectra between the two systems.

Figure 3 displays cuts of the estimated intensity of the magnetic scattering ($S_{\text{mag}}^{\text{Ce}}$) versus energy transfer. The magnetic contribution for $E_i = 60$ meV is obtained by subtracting an estimate of the phonon contribution of LaNiSnD$_{1.8}$ using

$$S_{\text{mag}}^{\text{Ce}}(\omega) = S_{\text{low}}^{\text{Ce}}(\omega) - S_{\text{high}}^{\text{Ce}}(\omega)\left[S_{\text{low}}^{\text{La}}(\omega)/S_{\text{high}}^{\text{La}}(\omega)\right], \quad (2)$$

where the S_{low} and S_{high} correspond to cuts integrated over low and high $|\mathbf{Q}|$, respectively. For $E_i = 20$ meV, the high-$|\mathbf{Q}|$ data of LaNiSnD$_{1.8}$ have relatively poor statistics, and therefore the magnetic contribution was estimated via directly subtracting the data of LaNiSnD$_{1.8}$ using

$$S_{\text{mag}}^{\text{Ce}}(\omega) = S_{\text{low}}^{\text{Ce}}(\omega) - \alpha S_{\text{low}}^{\text{La}}(\omega), \quad (3)$$

where $\alpha = 0.835$ is the ratio of the total neutron scattering cross sections per formula unit of CeNiSnD$_{1.8}$ and LaNiSnD$_{1.8}$. These data support there being CEF excitations at around 5 and 27 meV in CeNiSnD$_{1.8}$. In the hexagonal crystal structure of CeNiSnD$_{1.8}$ with space group $P6_3/mmc$ (No. 194), the Ce ions have trigonal point symmetry (D$_{3d}$) [42,45], and therefore the corresponding CEF Hamiltonian (H_{CEF}) has the form

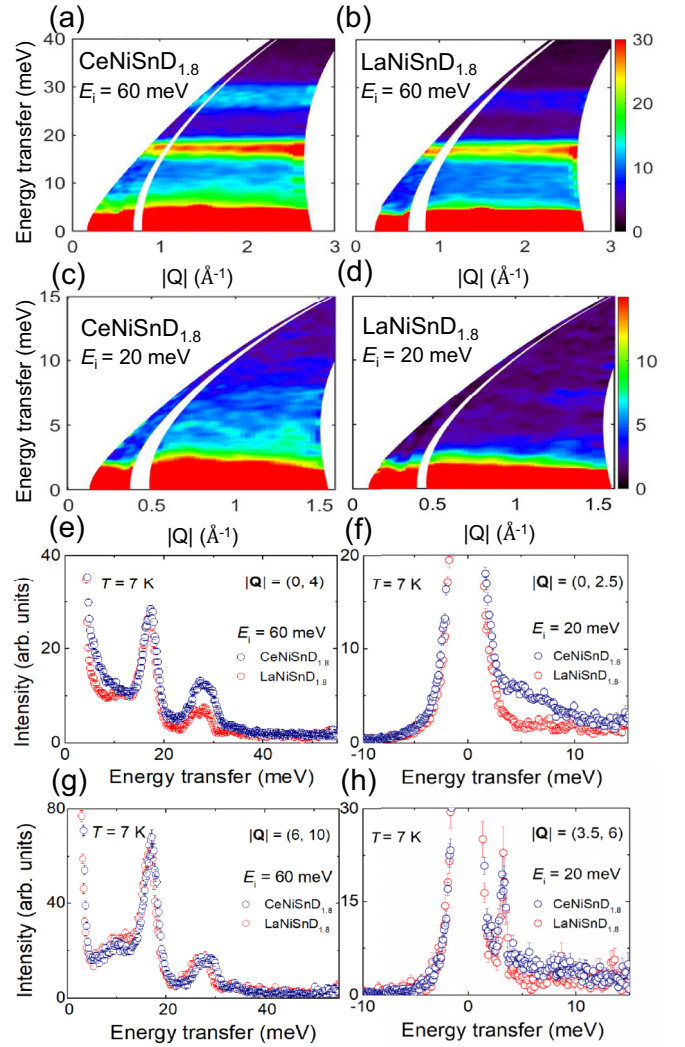$$H_{\text{CEF}} = B_2^0 O_2^0 + B_4^0 O_4^0 + B_4^3 O_4^3, \quad (4)$$

FIG. 2. Color plots of the inelastic neutron scattering response in the low angle banks as a function of energy transfer E and momentum transfer $|\mathbf{Q}|$ for (a) CeNiSnD$_{1.8}$ at 7 K ($E_i = 60$ meV), (b) LaNiSnD$_{1.8}$ at 7 K ($E_i = 60$ meV), (c) CeNiSnD$_{1.8}$ at 7 K ($E_i = 20$ meV), and (d) LaNiSnD$_{1.8}$ at 7 K ($E_i = 20$ meV). Cuts of the scattering intensity of CeNiSnD$_{1.8}$ and LaNiSnD$_{1.8}$ at 7 K vs E obtained from integrating across low $|\mathbf{Q}|$ in the range (e) 0–4 Å^{-1} with $E_i = 60$ meV, and (f) 0–2.5 Å^{-1} with $E_i = 20$ meV. Corresponding high-$|\mathbf{Q}|$ cuts are also displayed in the range (g) 6–10 Å^{-1} with $E_i = 60$ meV, and (h) 3.5–6 Å^{-1} with $E_i = 20$ meV. Note that for $E_i = 60$ meV, the low angle banks of the HET spectrometer reach a maximum momentum transfer of 3 Å^{-1} for energy transfers below 40 meV, but to around 4 Å^{-1} at higher energies.

where B_n^m are Stevens parameters and O_n^m are the Stevens operator equivalents [46]. As shown by the solid lines in Fig. 3, the data can be well fitted by this CEF model. Here, the 7 K data with both $E_i = 60$ meV and 20 meV were simultaneously fitted to obtain the CEF parameters. These parameters were then fixed in order to fit the $E_i = 20$ meV data at 50 and 100 K, which are also well described by this model. The obtained parameters are $B_2^0 = 0.802$ meV, $B_4^0 = 0.022$ meV, and $B_4^3 = -1.237$ meV. This gives rise to three doublets, where the energy differences between the ground state and the two
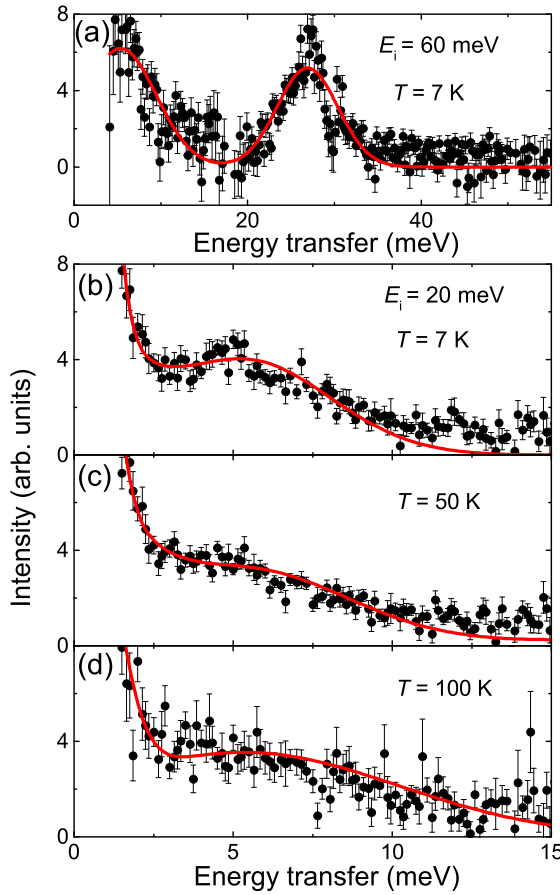
FIG. 3. Estimated magnetic contribution to the inelastic neutron scattering intensity of CeNiSnD$_{1.8}$ for (a) $E_i = 60$ meV at 7 K, (b) $E_i = 20$ meV at 7 K, (c) $E_i = 20$ meV at 50 K, and (d) $E_i = 20$ meV at 100 K. The solids lines show a fit to the CEF model described in the text.

excited levels are 5.34 and 26.91 meV and the corresponding wave functions of the three doublets are shown in Table II. Here, the wave function of the ground-state doublet ($|m_J\rangle$) is $|\psi^\pm\rangle = -0.863|\pm\frac{1}{2}\rangle \pm 0.505|\mp\frac{5}{2}\rangle$.

These results contrast with the CEF scheme with a $|\frac{3}{2}\rangle$ ground state, proposed based solely on magnetization measurements of CeNiSnH$_{1.8}$ polycrystalline samples [42]. For such a CEF level scheme, only the out-of-plane magnetic moment is nonzero and the predicted splitting of the excited CEF states is too small to account for our INS results. On the other hand, for our CEF scheme, the predicted ground-state magnetic moments along the *c* axis and in the *ab* plane are $\mu_z = 0.23\mu_B$/Ce and $\mu_x = 0.96\mu_B$/Ce, respectively, and an expected magnetization of $0.73\mu_B$/Ce is calculated for a polycrystalline sample in a 5 T applied field, which is slightly larger than the observed value of 0.5–0.6μ_B/Ce [42,47]. Furthermore, our deduced CEF ground state predicts a magnetic moment within the *ab* plane, in contrast to the uniaxial anisotropy of the CEF scheme in Ref. [42], but experimental determinations of the ordered moment direction, either from neutron diffraction or characterization of single crystals, are still lacking.
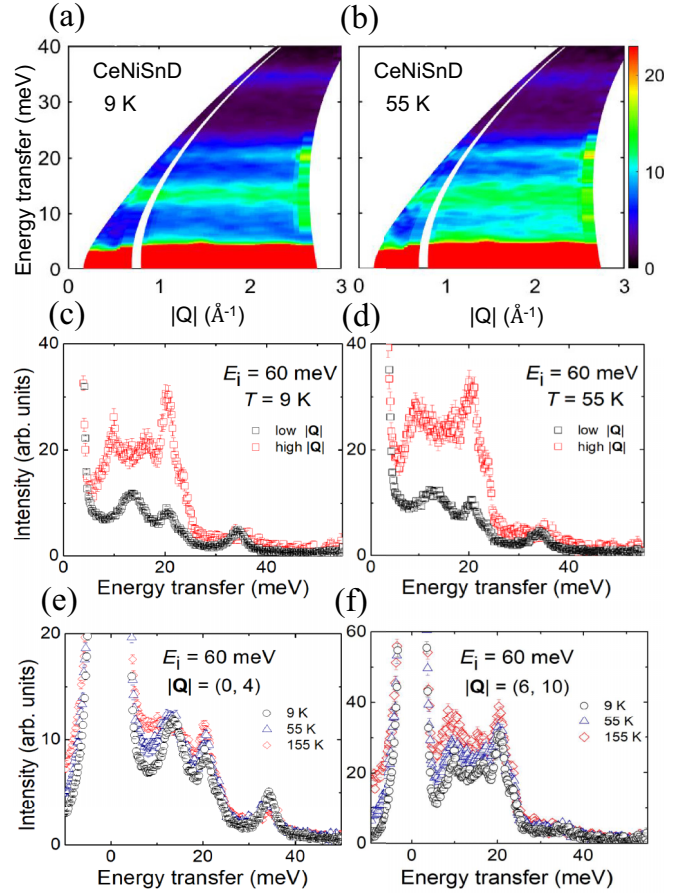

FIG. 4. Color-coded plot of the inelastic neutron scattering intensity in the low angle banks as a function of energy and momentum transfer for CeNiSnD at (a) 9 K and (b) 55 K, with $E_i = 60$ meV. The scattering intensity scale is in arbitrary units. Cuts of the neutron scattering intensity as a function of energy transfer obtained from integrating across a low-|**Q**| (0–4 Å^{-1}) and a high-|**Q**| (6–10 Å^{-1}) range for $E_i = 60$ meV at (c) 9 K and (d) 55 K. Cuts at various temperatures for $E_i = 60$ meV are displayed, obtained from integrating across (e) low-|**Q**| and (f) high-|**Q**| ranges.

2. CeNiSnD

Inelastic neutron scattering measurements were also performed on CeNiSnD at several temperatures above T_N with $E_i = 60$ meV in order to investigate the CEF excitations. Two-dimensional color plots of the scattering intensity versus *E* and |**Q**| at 9 and 55 K are displayed in Figs. 4(a) and 4(b), respectively. Corresponding cuts of the intensity of the data at the two temperatures integrated over low |**Q**| (0–4 Å^{-1}) and high |**Q**| (6–10 Å^{-1}) are displayed in Figs. 4(c) and 4(d). It can be seen in these cuts that at around 34 meV, there is a pronounced peak in the low-|**Q**| data of CeNiSnD that is absent at high |**Q**|. Meanwhile, while the high-|**Q**| data below 30 meV are larger than at low |**Q**| due to phonon contributions, there is also a peak in the low-|**Q**| data at around 13 meV that is absent at high |**Q**|. The intensity of these two magnetic excitations decreases with increasing temperature, as shown in Fig. 4(e), consistent with these corresponding to CEF excitations from the ground-state doublet to excited levels, while the peaks in the high-|**Q**| data increase at higher temperatures [Fig. 4(f)].
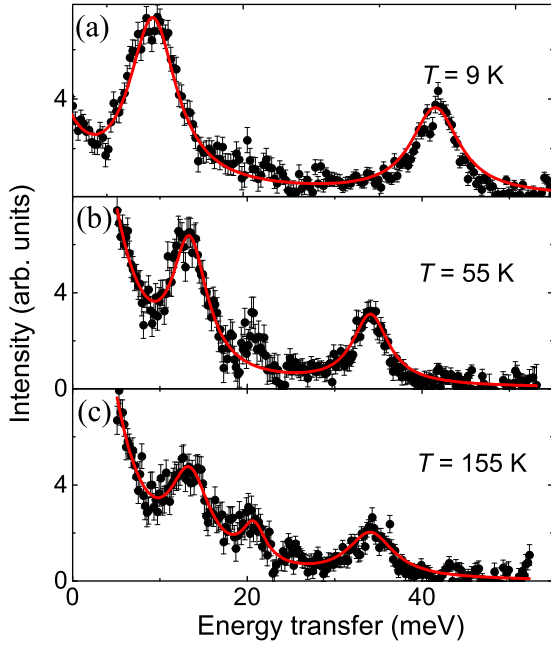
FIG. 5. Magnetic contribution to the inelastic neutron scattering intensity of CeNiSnD with $E_i = 60$ meV at (a) 9 K, (b) 55 K, and (c) 155 K. The solids lines show a fit to the CEF model described in the text. Note that there is some additional intensity at around 20 meV at 55 K, which likely corresponds to phonon scattering.

TABLE I. Crystal-electric field parameters $B_n^{\pm m}$ obtained from the analysis of the inelastic neutron scattering data of CeNiSnD.

$B_n^{\pm m}$	Value (meV)
B_2^0	0.102
B_2^1	0.428
B_2^2	0.895
B_2^{-1}	−1.152
B_2^{-2}	−2.029
B_4^0	0.009
B_4^1	0.020
B_4^2	0.035
B_4^3	−0.098
B_4^4	−0.125
B_4^{-1}	−0.019
B_4^{-2}	−0.319
B_4^{-3}	−0.035
B_4^{-4}	−0.044

Moreover, it can be seen that with increasing temperature, the intensity of the magnetic scattering at around 21 meV also increases, suggesting that this corresponds to a transition between the first and second excited CEF levels, once there is sufficient thermal energy to populate the first excited state. Note that a peak close to this energy is still present at 9 K, which has a larger intensity at high $|\mathbf{Q}|$, suggesting that there is also a phonon excitation at similar energy transfers.

CeNiSnD crystallizes in an orthorhombic structure, which has the same crystal structure as CeNiSn besides the addition of D$^+$ ions. Therefore, in order to estimate the magnetic scattering from CeNiSnD, the data of nonmagnetic LaNiSn [36] were directly subtracted using Eq. (3) and are displayed in Fig. 5 at three temperatures. It can be seen that at 9 K, there are two pronounced peaks corresponding to the aforementioned CEF excitations at around 13 and 34 meV. Note, also, that some additional intensity can still be detected at around 20 meV, which is likely a result of an incomplete subtraction of the phonon contribution. Since CeNiSnD contains light D atoms, which are absent in nonmagnetic LaNiSn, it might be expected that the phonon spectra of these compounds should be similar at low energies, but there could be some difference at higher energies.

For Ce^{3+} in an orthorhombic CEF with local point-group symmetry C_1, the $J = 5/2$ ground-state multiplet is also expected to split into three Kramers doublets in the paramagnetic state. The corresponding Hamiltonian is given by

$$H_{\text{CEF}} = B_2^0 O_2^0 + B_2^{\pm 1} O_2^{\pm 1} + B_2^{\pm 2} O_2^{\pm 2} + B_4^0 O_4^0 + B_4^{\pm 1} O_4^{\pm 1}$$
$$+ B_4^{\pm 2} O_4^{\pm 2} + B_4^{\pm 3} O_4^{\pm 3} + B_4^{\pm 4} O_4^{\pm 4}. \quad (5)$$

Due to low point-group symmetry of the Ce ions, there are a large number of CEF parameters $B_n^{\pm m}$ with 14 independent CEF parameters, which could not be uniquely determined from the observed spectra with two CEF excitations. Therefore, we fitted the data with an initial set of parameters corresponding to a point charge model with CEF excitations very close to those observed [48]. Using these initial parameters, the magnetic scattering at 9, 55, and 155 K were simultaneously fitted, and the resulting parameters are shown in Table I. It can be seen that this model can well fit the data, where there are excitations from the ground-state to excited state doublets at 13.4 and 34.1 meV, while at high temperatures, there is an addition excitation corresponding to the transition between the first and second excited states. The corresponding wave functions of the three doublets are shown in Table II. Based on this CEF scheme, the simulated magnetization predicts the c axis being the easy axis with a saturated moment of $1.26\mu_B$/Ce, which is consistent with the observed c-axis ordered moment of $1.37\,\mu_B$/Ce deduced from neutron diffraction [41]. However, given the large number of CEF parameters, this can only be regarded as a possible CEF scheme, and further measurements would be necessary to further constrain the CEF parameters, such as polarized neutron scattering on single-crystal samples, as performed for CePtSn [49].

IV. SUMMARY

We probed powder samples of CeNiSnD and CeNiSnD$_{1.8}$ using zero-field muon spin relaxation and inelastic neutron scattering measurements. μSR measurements of CeNiSnD confirm the presence of long-range magnetic order, whereby the whole sample undergoes a magnetic transition below $T_N = 4.7$ K. Moreover, the inelastic neutron scattering measurements reveal the presence of two well-defined CEF excitations in both compounds, at around 13 and 34 meV in CeNiSnD, and 5 and 27 meV for CeNiSnD$_{1.8}$. This is in contrast to CeNiSn, where evidence is found for a weak, broad, possible CEF excitation near 40 meV [34,35]. These results, therefore, suggest that the insertion of deuterium to

TABLE II. Energy levels and associated wave functions obtained from the analysis of the neutron scattering data of $CeNiSnD_{1.8}$ and CeNiSnD using a CEF model.

$CeNiSnD_{1.8}$	
Energy levels (meV)	Wave functions
0	$-0.863|\pm\frac{1}{2}\rangle \pm 0.505|\mp\frac{5}{2}\rangle$
5.338	$|\pm\frac{3}{2}\rangle$
26.909	$0.505|\mp\frac{1}{2}\rangle \mp 0.863|\pm\frac{5}{2}\rangle$
CeNiSnD	
Energy levels (meV)	Wave functions
0	$0.681|-\frac{5}{2}\rangle+(0.008+i0.144)|-\frac{3}{2}\rangle-(0.210+i0.664)|-\frac{1}{2}\rangle-(0.035+i0.006)|\frac{1}{2}\rangle+(0.121+i0.117)|\frac{3}{2}\rangle$
0	$(-0.158+i0.057)|-\frac{3}{2}\rangle-(0.034+i0.008)|-\frac{1}{2}\rangle+(0.463-i0.521)|\frac{1}{2}\rangle+(0.066-i0.128)|\frac{3}{2}\rangle-(0.622+i0.278)|\frac{5}{2}\rangle$
13.385	$(0.869+i0.242)|-\frac{3}{2}\rangle+(0.122+i0.017)|-\frac{1}{2}\rangle+(0.110-i0.213)|\frac{1}{2}\rangle+(-0.202+i0.174)|\frac{3}{2}\rangle+(0.084-i0.193)|\frac{5}{2}\rangle$
13.385	$-0.211|-\frac{5}{2}\rangle+(-0.240+i0.116)|-\frac{3}{2}\rangle-(0.239-i0.016)|-\frac{1}{2}\rangle+(0.029-i0.109)|\frac{1}{2}\rangle+(-0.125+i0.894)|\frac{3}{2}\rangle$
34.098	$(-0.168+i0.141)|-\frac{3}{2}\rangle+(-0.030+i0.040)|-\frac{1}{2}\rangle-(0.636+i0.190)|\frac{1}{2}\rangle-(0.097+i0.089)|\frac{3}{2}\rangle+(0.063-i0.698)|\frac{5}{2}\rangle$
34.098	$0.701|-\frac{5}{2}\rangle-(0.080+i0.105)|-\frac{3}{2}\rangle+(0.132+i0.650)|-\frac{1}{2}\rangle+(0.042-i0.027)|\frac{1}{2}\rangle-(0.155-i0.155)|\frac{3}{2}\rangle$

CeNiSn decreases the hybridization between the $4f$ electrons and the conduction electrons, leading to the localization of the $4f$ electrons, together with the occurrence of long-range magnetic order. This is consistent with the lack of magnetic order in CeNiSn being a consequence of the strong Kondo hybridization [38,50], rather than there being a disordered arrangement of local moments. The 40 meV excitation in CeNiSn is slightly higher in energy than the second excited level of isostructural CeNiSnD, suggesting that the CEF potential is either modified by the presence of deuterium ions or the different nature of the conduction electrons. A CEF model for the trigonal local symmetry of the Ce ion can well account for the magnetic scattering of $CeNiSnD_{1.8}$, for which the predicted moment for the resulting ground state is $0.96\mu_B/Ce$ within the *ab* plane, and the observed magnetization for a polycrystalline sample is similar to that expected for the CEF model [42,47]. However, determining whether there is a reduced ordered moment arising from Kondo coupling between the $4f$ and conduction electrons requires further characterization of the magnetic ground state of $CeNiSnD_{1.8}$. Meanwhile, we propose a tentative CEF model for CeNiSnD, for which the saturated moment along the easy *c* axis of $1.26\mu_B/Ce$ is also similar to that deduced from neutron diffraction [41], but the low symmetry of the Ce site means that additional measurements would be necessary to constrain the CEF parameters.

[1] Q. Si and F. Steglich, Heavy fermions and quantum phase transitions, Science **329**, 1161 (2010).

[2] C. Pfleiderer, Superconducting phases of f-electron compounds, Rev. Mod. Phys. **81**, 1551 (2009).

[3] Z. F. Weng, M. Smidman, L. Jiao, X. Lu, and H. Q. Yuan, Multiple quantum phase transitions and superconductivity in Ce-based heavy fermions, Rep. Prog. Phys. **79**, 094503 (2016).

[4] T. Mahon, S. Tencé, R. Pöttgen, B. Chevalier, and E. Gaudin, Study of the structural transition and hydrogenation of CeTiGe, J. Alloys Compd. **805**, 701 (2019).

[5] E. Gaudin, B. Chevalier, W. Hermes, U. C. Rodewald, and R. Pöttgen, Structure, magnetic and electrical properties of CeIrSb and its hydride CeIrSbH$_{0.8}$, J. Solid State Chem. **182**, 1827 (2009).

[6] B. Chevalier, E. Gaudin, S. Tencé, B. Malaman, J. R. Fernandez, G. André, and B. Coqblin, Hydrogenation inducing antiferromagnetism in the heavy-fermion ternary silicide CeRuSi, Phys. Rev. B **77**, 014414 (2008).

[7] B. Chevalier, A. Wattiaux, and J.-L. Bobet, The Doniach diagram and hydrogenation of the ternary compounds CePdIn and CePdSn, J. Phys.: Condens. Matter **18**, 1743 (2006).

[8] B. Chevalier, W. Hermes, B. Heying, U. C. Rodewald, A. Hammerschmidt, S. F. Matar, E. Gaudin, and R. Pöttgen, New hydrides REScSiH and REScGeH (RE = La, Ce): Structure, magnetism, and chemical bonding, Chem. Mater. **22**, 5013 (2010).

[9] B. Chevalier and S. F. Matar, Effect of H insertion on the magnetic, electronic, and structural properties of CeCoSi, Phys. Rev. B **70**, 174408 (2004).

[10] B. Chevalier, S. Matar, J. Sanchez Marcos, and J. Rodriguez Fernandez, From antiferromagnetic ordering to spin fluctuation behavior induced by hydrogenation of ternary compounds CeCoSi and CeCoGe, Phys. B: Condens. Matter **378-380**, 795 (2006).

[11] B. Chevalier, E. Gaudin, F. Weill, and J.-L. Bobet, Hydrogenation and physical properties of the ternary germanide CeCoGe: An anisotropic expansion of the unit cell, Intermetallics **12**, 437 (2004).

[12] T. Mahon, E. Gaudin, A. Villesuzanne, R. Decourt, J.-L. Bobet, O. Isnard, B. Chevalier, and S. Tencé, Hydrogen insertion in the intermetallic GdScGe: A drastic reduction of the dimensionality of the magnetic and transport properties, Inorg. Chem. **57**, 14230 (2018).

[13] T. Takabatake, F. Teshima, H. Fujii, S. Nishigori, T. Suzuki, T. Fujita, Y. Yamaguchi, J. Sakurai, and D. Jaccard, Formation of an anisotropic energy gap in the valence-fluctuating system of CeNiSn, Phys. Rev. B **41**, 9607(R) (1990).

[14] T. Takabatake, M. Nagasawa, H. Fujii, G. Kido, M. Nohara, S. Nishigori, T. Suzuki, T. Fujita, R. Helfrich, U. Ahlheim, K. Fraas, C. Geibel, and F. Steglich, Anisotropic suppression of the energy gap in CeNiSn by high magnetic fields, Phys. Rev. B **45**, 5740 (1992).

[15] G. Nakamoto, T. Takabatake, H. Fujii, A. Minami, K. Maezawa, I. Oguro, and A. Menovsky, Crystal growth and characterization of the Kondo semimetal CeNiSn, J. Phys. Soc. Jpn. **64**, 4834 (1995).

[16] K. Izawa, T. Suzuki, T. Fujita, T. Takabatake, G. Nakamoto, H. Fujii, and K. Maezawa, Metallic ground state of CeNiSn, Phys. Rev. B **59**, 2599 (1999).

[17] T. Ekino, T. Takabatake, H. Tanaka, and H. Fujii, Tunneling evidence for the quasiparticle gap in Kondo semiconductors CeNiSn and CeRhSb, Phys. Rev. Lett. **75**, 4262 (1995).

[18] M. Kyogaku, Y. Kitaoka, H. Nakamura, K. Asayama, T. Takabatake, F. Teshima, and H. Fujii, NMR investigation of energy Gap formation in the valence fluctuating compound CeNiSn, J. Phys. Soc. Jpn. **59**, 1728 (1990).

[19] K. Nakamura, Y. Kitaoka, K. Asayama, T. Takabatake, H. Tanaka, and H. Fujii, Low-energy excitation in Kondo semiconductors CeNiSn and CeRhSb, J. Phys. Jpn. **63**, 433 (1994).

[20] U. Stockert, P. Sun, N. Oeschler, F. Steglich, T. Takabatake, P. Coleman, and S. Paschen, Giant isotropic nernst effect in an anisotropic Kondo semimetal, Phys. Rev. Lett. **117**, 216401 (2016).

[21] H. Ikeda and K. Miyake, A theory of anisotropic semiconductor of heavy fermions, J. Phys. Soc. Jpn. **65**, 1769 (1996).

[22] J. Moreno and P. Coleman, Gap-anisotropic model for the narrow-gap Kondo insulators, Phys. Rev. Lett. **84**, 342 (2000).

[23] M. Kyogaku, Y. Kitaoka, H. Nakamura, K. Asayama, T. Takabatake, F. Teshima, and H. Fujii, NMR study of quasiparticle gap in CeNiSn, Phys. B: Condens. Matter **171**, 235 (1991).

[24] P.-Y. Chang, O. Erten, and P. Coleman, Möbius Kondo insulators, Nat. Phys. **13**, 794 (2017).

[25] T. Yoshida, A. Daido, N. Kawakami, and Y. Yanase, Efficient method to compute $\mathbb{Z}_4$ indices with glide symmetry and applications to the Möbius materials CeNiSn and UCoGe, Phys. Rev. B **99**, 235105 (2019).

[26] T.-S. Nam, C.-J. Kang, D.-C. Ryu, J. Kim, H. Kim, K. Kim, and B. I. Min, Topological bulk band structures of the hourglass and Dirac nodal-loop types in Ce Kondo systems: CeNiSn, CeRhAs, and CeRhSb, Phys. Rev. B **99**, 125115 (2019).

[27] S. Seong, J. D. Denlinger, K. Kim, B. I. Min, Y. Ōnuki, and J.-S. Kang, Hourglass-type bulk Ni $3d$ band and Ce $4f$ Kondo resonance states in the potential topological Kondo semimetal CeNiSn via angle-resolved photoemission spectroscopy, Phys. Rev. B **107**, 125109 (2023).

[28] T. E. Mason, G. Aeppli, A. P. Ramirez, K. N. Clausen, C. Broholm, N. Stücheli, E. Bucher, and T. T. M. Palstra, Spin gap and antiferromagnetic correlations in the Kondo insulator CeNiSn, Phys. Rev. Lett. **69**, 490 (1992).

[29] H. Kadowaki, T. Sato, H. Yoshizawa, T. Ekino, T. Takabatake, H. Fujii, L. P. Regnault, and Y. Isikawa, Quasi-one-dimensional antiferromagnetic correlation in the kondo semiconductor CeNiSn, J. Phys. Soc. Jpn. **63**, 2074 (1994).

[30] T. J. Sato, H. Kadowaki, H. Yoshizawa, T. Ekino, T. Takabatake, H. Fujii, L. P. Regnault, and Y. Isikawa, Neutron scattering study of antiferromagnetic correlations in the Kondo semiconductor CeNiSn, J. Phys.: Condens. Matter **7**, 8009 (1995).

[31] S. Raymond, L. P. Regnault, T. Sato, H. Kadowaki, N. Pyka, G. Nakamoto, T. Takabatake, H. Fujii, Y. Isikawa, G. Lapertot, and J. Flouquet, An inelastic neutron scattering study of the Kondo semiconductor CeNiSn in high magnetic field, J. Phys.: Condens. Matter **9**, 1599 (1997).

[32] Y. Kagan, K. A. Kikoin, and N. V. Prokof'ev, Nature of the pseudogap in the energy spectrum of CeNiSn, JETP Lett. **57**, 600 (1993).

[33] Y. Kagan, K. A. Kikoin, and A. S. Mishchenko, Interplay between heavy fermions and crystal-field excitation in Kondo lattices: Low-temperature thermodynamics and inelastic neutron scattering spectra of CeNiSn, Phys. Rev. B **55**, 12348 (1997).

[34] J.-G. Park, D. Adroja, K. McEwen, Y. Bi, and J. Kulda, Crystal field excitation of single crystal CeNiSn, Phys. B: Condens. Matter **259-261**, 288 (1999).

[35] J.-G. Park, D. T. Adroja, K. A. McEwen, Y. J. Bi, and J. Kulda, Possible crystal-field excitation in single-crystal CeNiSn, Phys. Rev. B **58**, 3167 (1998).

[36] J.-Y. So, S.-J. Oh, J.-G. Park, D. T. Adroja, K. A. McEwen, and T. Takabatake, Inelastic neutron scattering studies of doped CeNiSn and CeRhSb: Crystal-field excitations and origin of the pseudogap, Phys. Rev. B **71**, 214441 (2005).

[37] M. Kohgi, K. Ohoyama, T. Osakabe, and M. Kasaya, Neutron scattering studies of CeTSn (T = Ni, Pd), J. Magn. Magn. Mater. **108**, 187 (1992).

[38] D. Adroja, B. Rainford, A. Neville, and A. Jansen, Crossover from antiferromagnetic Kondo metal to Kondo insulator in Ce(Pt$_{1-x}$Ni$_x$)Sn alloys, Phys. B: Condens. Matter **223-224**, 275 (1996).

[39] B. Chevalier, M. Pasturel, J.-L. Bobet, J. Etourneau, O. Isnard, J. Sanchez Marcos, and J. Rodriguez Fernandez, Magnetic ordering induced by the hydrogenation of the ternary stannide CeNiSn, J. Magn. Magn. Mater. **272-276**, 576 (2004).

[40] J. Sánchez Marcos, J. Rodríguez Fernández, and B. Chevalier, Hydrogen induced antiferromagnetism in CeNiSn studied by heat capacity and magnetocaloric effect, J. Magn. Magn. Mater. **310**, 383 (2007).

[41] V. Yartys, B. Ouladdiaf, O. Isnard, O. Khyzhun, and K. Buschow, Hydrogen induced antiferromagnetism in the Kondo semimetal CeNiSn, J. Alloys Compd. **359**, 62 (2003).

[42] B. Chevalier, J.-L. Bobet, M. Pasturel, E. Bauer, F. Weill, R. Decourt, and J. Etourneau, Ferromagnetic behavior of the new hydride CeNiSnH$_{1.8(2)}$, Chem. Mater. **15**, 2181 (2003).

[43] O. Arnold, J. Bilheux, J. Borreguero, A. Buts, S. Campbell, L. Chapon, M. Doucet, N. Draper, R. Ferraz Leal, M. Gigg, V. Lynch, A. Markvardsen, D. Mikkelson, R. Mikkelson, R. Miller, K. Palmen, P. Parker, G. Passos, T. Perring, P. Peterson *et al.*, Mantid-data analysis and visualization package for neutron scattering and μSR experiments, Nucl. Instrum. Methods Phys. Res., Sect. A **764**, 156 (2014).

[44] O. Isnard, C. Rusu, R. Dudric, D. Andreica, A. Amato, and B. Chevalier, Low-temperature and high-pressure μSR study of the strongly correlated CeNiSnH$_x$ compounds, Phys. Rev. B **93**, 224424 (2016).

[45] B. Chevalier, A. Wattiaux, L. Fournès, and M. Pasturel, ^{119}Sn Mössbauer spectroscopy studies of hydrides deriving from the stannide CeNiSn, Solid State Sci. **6**, 573 (2004).

[46] K. W. H. Stevens, Matrix elements and operator equivalents connected with the magnetic properties of rare earth ions, Proc. Phys. Soc. Sec. A **65**, 209 (1952).

[47] J. R. Fernandez, S. F. Matar, D. P. Rojas, L. Torralbo-Campo, and B. Chevalier, Influence of pressure on the magnetic ordering of CeNiSnH and CeNiSnH$_{1.8}$ hydrides, J. Phys.: Condens. Matter **21**, 305601 (2009).

[48] V. K. Anand, D. T. Adroja, C. Ritter, D. Das, H. S. Nair, A. Bhattacharyya, L. Liborio, S. Sturniolo, F. L. Pratt, D. Le, G. Andre, H. Luetkens, A. D. Hillier, and Z. Hossain, Magnetic structure and crystal field states of Pr$_2$Pd$_3$Ge$_5$: μSR and neutron scattering investigations, Phys. Rev. B **107**, 104412 (2023).

[49] B. Janoušová, J. Kulda, M. Diviš, V. Sechovský, and T. Komatsubara, Local symmetry of the crystal-field Hamiltonian of CePtSn by polarized neutron scattering, Phys. Rev. B **69**, 220412(R) (2004).

[50] M. Kasaya, T. Tani, H. Suzuki, K. Ohoyama, and M. Kohgi, Crossover from magnetic to nonmagnetic ground state in the Kondo alloy system Ce(Ni$_{1-x}$Pd$_x$)Sn, J. Phys. Soc. Jpn. **60**, 2542 (1991).